SCIENTIFIC REPORTS

OPEN

SUBJECT AREAS:
QUANTUM OPTICS
NANOPHOTONICS AND PLASMONICS
QUANTUM DOTS
NANOCAVITIES

Received
18 February 2013

Accepted
19 February 2013

Published
7 March 2013

Correspondence and requests for materials should be addressed to S.A. (serkan.ates@nist.gov) or K.S. (kartik.srinivasan@nist.gov)

Improving the performance of bright quantum dot single photon sources using temporal filtering via amplitude modulation

Serkan Ates[1,2], Imad Agha[1,2], Angelo Gulinatti[3], Ivan Rech[3], Antonio Badolato[4] & Kartik Srinivasan[1]

[1]Center for Nanoscale Science and Technology, National Institute of Standards and Technology, Gaithersburg, MD 20899, USA, [2]Maryland NanoCenter, University of Maryland, College Park, MD 20742, USA, [3]Politecnico di Milano, Dipartimento di Elettronica e Informazione, Piazza da Vinci 32, 20133 Milano, Italy, [4]Department of Physics and Astronomy, University of Rochester, Rochester, NY 14627, USA.

Single epitaxially-grown semiconductor quantum dots have great potential as single photon sources for photonic quantum technologies, though in practice devices often exhibit nonideal behavior. Here, we demonstrate that amplitude modulation can improve the performance of quantum-dot-based sources. Starting with a bright source consisting of a single quantum dot in a fiber-coupled microdisk cavity, we use synchronized amplitude modulation to temporally filter the emitted light. We observe that the single photon purity, temporal overlap between successive emission events, and indistinguishability can be greatly improved with this technique. As this method can be applied to any triggered single photon source, independent of geometry and after device fabrication, it is a flexible approach to improve the performance of systems based on single solid-state quantum emitters, which often suffer from excess dephasing and multi-photon background emission.

Solid-state quantum emitters are potentially bright, stable, and monolithic sources of triggered single photons for scalable photonic quantum information technology[1,2]. Source properties which must be optimized for applications include the fraction of photons emitted into a useful optical channel, the repetition rate at which the source is operated, the degree to which multi-photon emission is suppressed, and the extent to which the single photons are identical. One specific solid-state system that has drawn considerable interest is the InAs/GaAs quantum dot (QD) heterostructure. Despite significant development of these sources, achieving good performance with respect to all of the aforementioned parameters can be challenging[3,4]. For example, the high refractive index contrast between GaAs and air requires modification of the geometry to prevent most of the QD emission from remaining trapped within the semiconductor. The existence of radiative states within the QD heterostructure that are spectrally resonant with the transition of interest can limit the single photon purity of the emission. Interactions between the excitonic transition and electronic carriers and phonons in the host semiconductor can cause dephasing that prevents the emitted photons from being perfectly indistinguishable.

Researchers have developed a number of tools to address these limitations. Nanofabricated photonic structures can ensure that a significant fraction of the QD emission is collected[5–10]. Optical excitation resonant with excited states of the QD can limit multi-photon emission[11], increase the coherence time, and improve the degree of indistinguishability[12–14]. Purcell-enhancement of the radiative rate through modification of the QD's electromagnetic environment[15] can also produce single photon wavepackets that are more indistinguishable[12,14,16]; furthermore, it increases the maximum repetition rate at which the source can be operated.

Here, we describe a different approach to improving the performance of QD single photon sources (SPSs). Rather than influencing the QD radiative dynamics, we instead use temporal filtering through electro-optic amplitude modulation to process and purify the QD emission. Synchronized modulation of single photon wavepackets has recently been demonstrated for both atomic[17,18] and QD systems[19], but those works focused primarily on demonstrating that modulation was possible and the variety of wavepacket shapes that it could produce. We begin by demonstrating a bright, fiber-coupled SPS ($>$ 20% overall collection efficiency into the fiber) based on a QD in a microdisk cavity, and then show that the ability to temporally select portions of the

emitted signal can lead to large improvements in the purity and indistinguishability of the source. In particular, we demonstrate an improvement in the single photon purity by a factor as high as 8, enough temporal separation between successive emission events to achieve a 0.5 GHz repetition rate source, and an improvement in the two-photon wavepacket overlap by a factor of 2. In contrast to other approaches which require modification of the source, this technique can be applied to any existing solid-state triggered SPS, regardless of the device geometry and excitation method (optical or electrical), and can thus be a versatile resource when implementing solid-state SPSs in quantum information applications.

Results

Efficient fiber-coupled single photon source. We use a self-assembled InAs QD embedded in a GaAs microdisk cavity (Fig. 1a) as a triggered SPS. Our main objective is to produce a bright source under pulsed excitation. We use relatively small diameter ($D \sim 2.9\,\mu$m) devices to obtain a high QD spontaneous emission coupling fraction β into the resonant whispering gallery modes (WGMs) of the microdisk. Efficient outcoupling of the WGMs is achieved using a fiber taper waveguide (FTW), an approach previously used to create fiber-coupled microdisk-quantum-dot lasers[20] and waveguide SPSs[21]. Out-coupling of a WGM through the FTW is quantified by an efficiency η, whose value is experimentally determined by measuring the transmission spectrum of the cavity [see Supplementary Information]. The overall collection efficiency of photons into each channel of the FTW is $\xi = \beta\eta$, in the limit of unity QD radiative efficiency.

The setup shown in Fig. 1b is used to measure the low-temperature micro-photoluminescence spectrum of a microdisk-QD device shown in Fig. 1c, where a bright excitonic line is observed on top of a broad cavity mode at 969 nm. The relatively low quality factor mode (Q = 1900; see inset transmission spectrum) results in a Purcell factor $F_P = 2$, as determined by measuring the emission lifetime when the QD is on-resonance with the mode and far-detuned from it (inset to Fig. 1c). The brightness of the QD source is determined through the excitation power-dependent intensity of the filtered signal, which is directly measured with a Si single-photon avalanche diode (SPAD), as shown in Fig. 1d. The right vertical axis is the measured count rate at the detector, while the left axis is the photon count rate coupled to the forward channel of the FTW, factoring in the losses due to spectral filtering, detection efficiency of the SPAD, and the transmission of the FTW (see Methods). At saturation, a collection efficiency $\xi = 11.9\% \pm 0.6\%$ into the forward channel of the FTW is estimated. Ideally, collection into the backward channel will equal that into the forward channel; for this device, we measure a slight reduction (by 14%) in the backward channel (inset of Fig. 1d), most likely due to asymmetric losses in the setup. This yields $\xi = 10.2\% \pm 0.6\%$ for the backward channel, so that if both channels are combined, the overall collection efficiency into the FTW is $\approx 22\%$.

The single-photon nature of the collected QD emission is demonstrated by measuring the second-order photon correlation function $g^{(2)}(\tau)$ using a Hanbury-Brown and Twiss (HBT) setup [see Supplementary Information for details]. Even at P_{sat}, the pump power for which the emission is highest, we observe (upper panel of Fig. 1e) a clear suppression of the correlation peak at zero time delay, with $g^{(2)}(0) = 0.16 \pm 0.01 < 0.5$. We also characterize the indistinguishability of the single photon emission using a Hong-Ou-Mandel (HOM) interferometer[12,22], where consecutively emitted photons are overlapped on a beamsplitter. As discussed in Ref. 12 and in the Supplementary Information, the degree of indistinguishability

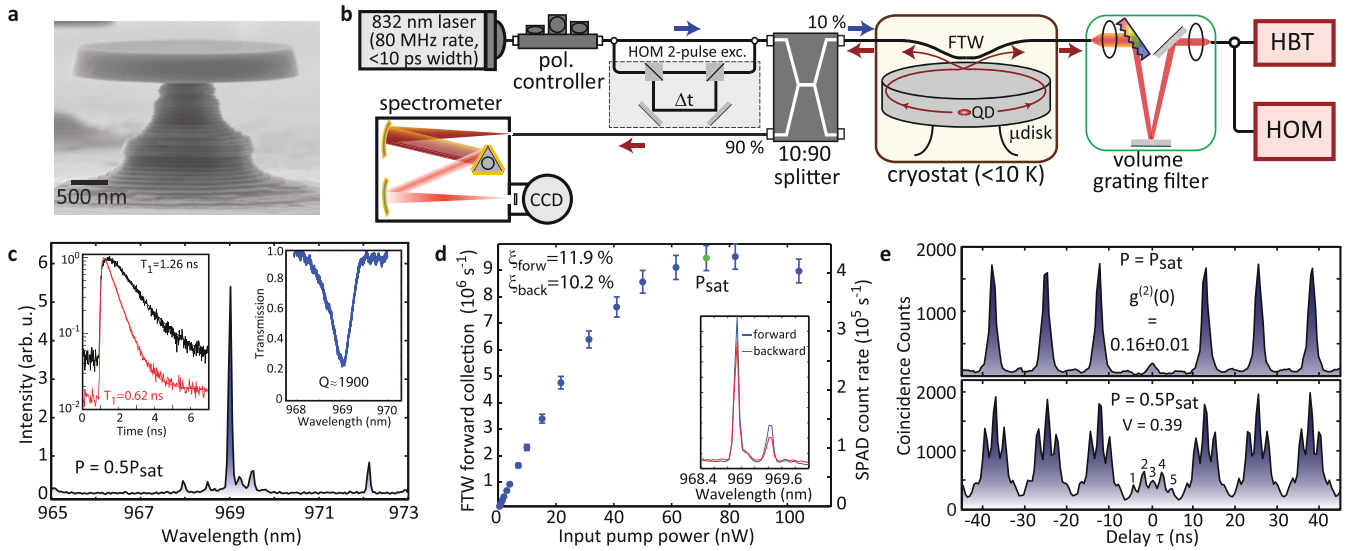

Figure 1 | Bright, fiber-coupled microcavity-QD single photon source. (a) Scanning electron microscope image of the GaAs microdisk cavity. (b) Experimental setup [details in the Supplementary Information]. The 10:90 directional coupler allows for simultaneous measurement of the forward and backward channels of the FTW. Typically, the emission spectrum is monitored through the backward channel while the forward channel is spectrally filtered to select the desired QD transition, which is then used in subsequent photon correlation measurements. HBT = Hanbury-Brown and Twiss setup; HOM = Hong-Ou-Mandel interferometer. (c) Photoluminescence (PL) spectrum for a QD-microdisk device. The left inset shows the PL decay of the QD line at 969 nm, both when the cavity is detuned (black) and on-resonance (red). The right inset shows a transmission spectrum of the microdisk. (d) Spectrally-filtered QD emission as a function of pump power, where the right y-axis shows the detected count rate on a Si SPAD and the left *y*-axis shows the corresponding photon count rate collected into the forward direction of the FTW. P_{sat} is the pump power at which the QD emission is highest. The inset shows the measured PL spectrum from both the forward (blue) and backward (red) direction of the FTW. (e) Upper panel: Second-order correlation function measured at P_{sat}. Lower panel: Photon indistinguishability measurement. The suppression of peak 3 with respect to peaks 2 and 4 is due to the two-photon interference effect with $V = 0.39 \pm 0.05$ [see Supplementary Information]. Error bars in (d) come from the fluctuation in the detected count rates, and are one standard deviation values. The uncertainty in the $g^{(2)}(0)$ values is given by the standard deviation in the area of the peaks away from time zero, and leads to the uncertainty in *V*.

is experimentally related to $M = \frac{A_2}{A_2 + A_4}$, where $A_{2,3,4}$ are the areas of the peaks labeled in the lower panel of Fig. 1e. For our QD SPS with $g^{(2)}(0) = 0.16 \pm 0.01$ at $0.5P_{sat}$ (Fig. 2(d)), $M < 0.57$ can only occur if there is two-photon interference (see Methods). $M = 0.40$ is observed in Fig. 1e, indicating a degree of indistinguishability that is quantified by the two-photon wavepacket overlap $V = 0.39 \pm 0.05$.

Since β approaches 50% in these devices (half into each of the clockwise and counterclockwise modes), improving the brightness of this source requires an increase in η, which is estimated to be ≈25% in the current devices [see Supplementary Information]. This would require improved overlap between the FTW and microdisk WGMs, through adjustment of the microdisk and FTW dimensions. While the demonstrated brightness of ≈ 11% (22%) into one (both) channel (channels) of the fiber is smaller than the collection into the first optic in recent demonstrations[7,9], it has the advantages of being directly fiber-coupled, exhibiting Purcell enhancement with a relatively low $g^{(2)}(0)$ value at saturation, and having indistinguishability with a two-photon wavepacket overlap of 39%. Direct fiber coupling enables the source to be easily interfaced with other optical components and physical systems for more sophisticated experiments, as it ensures a high brightness of spectrally isolated photons in ubiquitously-used single mode optical fiber [more details in the Supplementary Information]. For example, recent quantum frequency conversion experiments involving a QD SPS have made use of such a source[23]. Here, we use this fiber optic interface to easily connect with an electro-optic amplitude modulator, which we use in the following sections to manipulate the purity, repetition rate, and indistinguishability of the QD SPS.

Improving the purity of the single photon source. A non-zero value of $g^{(2)}(0)$ is commonly measured in QD SPSs, and indicates the presence of temporally coincident multi-photon emission (within the timing resolution of the system). Such emission can originate from other spectrally-resonant radiative transitions in the system that arise due to the nature of the QD confinement, which supports a quasi-continuum of (multi)excitonic transitions whose emission can be enhanced by the presence of a cavity mode[24–26]. Another process that can lead to $g^{(2)}(0) > 0$ is carrier recapture on a time scale comparable to the QD radiative lifetime, which can enable the emission of more than one photon per excitation pulse[11,27,28]. In this section, we show how amplitude modulation can reduce the multi-photon contribution, thereby improving the purity of the QD SPS.

The modified setup is shown in Fig. 2a. The trigger output of the 832 nm excitation laser is used to synchronize an electronic pulse generator whose output drives a fiber-coupled, 980 nm band electro-optic modulator (EOM). Spectrally-filtered QD emission is fed into the EOM, and its output is sent to the HBT setup for photon correlation measurements. The pulse generator produces optical pulses of width $T_{mod} > 350$ ps, measured as the full-width at the 1/e point. The separation between the EOM gates and the incoming QD emission can be controlled with ps resolution.

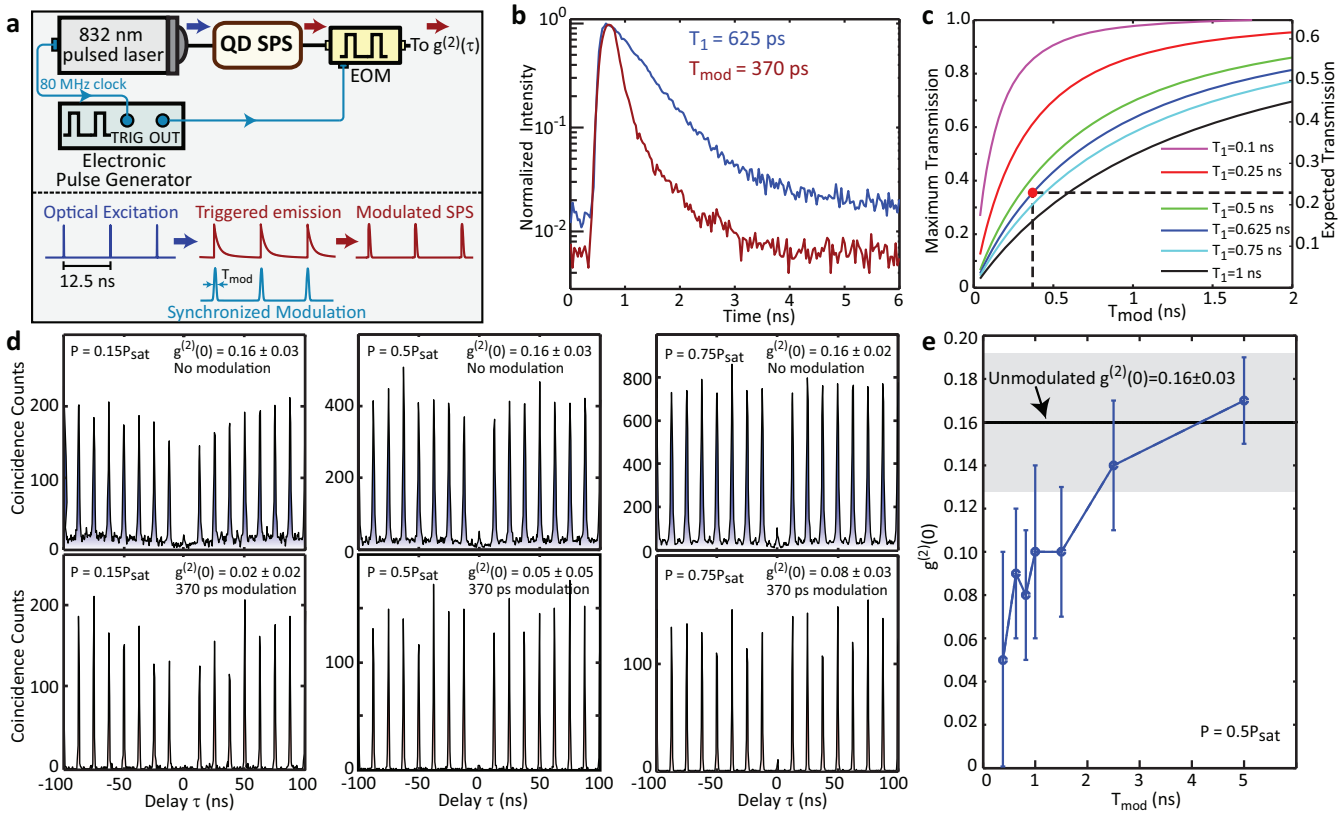

Figure 2 | Improved single photon purity using amplitude modulation. (a) Schematic of the amplitude modulation setup. EOM = electro-optic modulator. (b) QD lifetime traces under no modulation (blue) and 370 ps modulation (red). (c) Calculated transmission through the EOM as a function of modulation width T_{mod}, for varying T_1. The left y-axis shows the maximum possible transmission, while the right y-axis includes 1.9 dB of insertion loss through the EOM. The highlighted point is the expected transmission level assuming $T_1 = 625$ ps and for the 370 ps modulation used in subsequent experiments. (d) Pump-power-dependent second order correlation measurements, without modulation (top) and with modulation (bottom). (e) Modulation-width-dependent second order correlation measurement at $0.5P_{sat}$. The shaded gray region corresponds to $g^{(2)}(0) = 0.16 \pm 0.03$, measured for no modulation. The uncertainty in the $g^{(2)}(0)$ values in (d) and (e) is given by the standard deviation in the area of the peaks away from time zero.

Figure 2b shows the QD lifetime measured with and without amplitude modulation, where the modulation produces T_{mod} = 370 ps ± 20 ps, and its extinction level is >20 dB. Amplitude modulation is expected to reduce the overall source brightness, both through its temporal gating function and broadband insertion loss. The transmission through the temporal gate can be estimated by considering the overlap of the EOM response and the QD emission [see Supplementary Information]. Assuming that the EOM gate position is optimal and that the QD emission follows a decaying exponential, Fig. 2c shows the expected transmission level through the EOM for varying values of the radiative lifetime T_1 in the case of no insertion loss (left y-axis) and the measured 1.9 dB insertion loss (right y-axis). For the measured $T_1 \approx 625$ ps and $T_{mod} = 370$ ps, the maximum and expected transmission levels are 36% and 23%, respectively.

Amplitude modulated QD emission is then sent to the HBT setup, and $g^{(2)}(\tau)$ is measured as a function of excitation power, as shown in Fig. 2d, with the unmodulated $g^{(2)}(\tau)$ measurements provided for reference. A clear suppression in the $g^{(2)}(0)$ values after modulation is observed, with improvements ranging from a factor of eight at a pump power of $0.15P_{sat}$ to a factor of two at $0.75P_{sat}$. The measured count rates on the Si SPADs after modulation are typically ≈20% of the value before modulation.

The basic function of the modulator is to select a portion of the QD emission with a user-defined width and center position. Thus, if the desired single photon emission has a different width and/or temporal position with respect to multi-photon processes, the amplitude modulation can discriminate between the two, removing the undesired multi-photon emission. To gain a better understanding of how the timescale for single-photon and multi-photon emission differ in this device, we measure $g^{(2)}(0)$ as a function of T_{mod} at an excitation power of $0.5P_{sat}$, as shown in Fig. 2e and in the Supplementary Information. The nearly monotonic increase in $g^{(2)}(0)$ with increasing modulation width shows that in this device, multi-photon emission is spread over a timescale of a few ns.

The separation in timescales for single- and multi-photon emission most likely depends on specific characteristics of the device in question, including the pumping scheme and properties of the cavity mode and its detuning with respect to the QD exciton state. Recapture processes in the QD that lead to multiple photon emission events from the QD excitonic line within a single excitation pulse[11,27,28] represent one scenario in which such temporal separation may occur. Alternately, recent studies[25,26] have examined the differences in temporal behavior between single exciton and multi-excitonic transitions of the QD, and have observed that the emission processes can be delayed with respect to each other.

The temporal filtering provided by amplitude modulation can also be useful in QD SPSs that operate at higher repetition rates. For a source with pure single photon emission, the maximum repetition rate depends on the radiative dynamics of the QD, including the carrier capture time and QD radiative lifetime T_1. Purcell enhancement to shorten T_1[29] and rapid quenching of the QD emission at a timescale $< T_1$[30] have been used to approach GHz repetition rates. However, processes that lead to multi-photon emission can be a limitation. Considering the aforementioned carrier recapture processes, even if they still allow photons to be emitted one at a time, multiple emission events per excitation cycle will degrade the on-demand functionality of the source. Experimentally, researchers have attributed various features in $g^{(2)}(\tau)$ data to such processes[11,28]. For example, while measurements of QD SPSs under above-band excitation do exhibit a pronounced antibunching dip (because photons are emitted one-by-one), emission events that are asynchronous with the excitation trigger lead to an overall background in $g^{(2)}(\tau)$ at other times. Such behavior is exhibited in our data without amplitude modulation (upper graphs in Fig. 2d), and suggests that a higher repetition rate source would benefit from suppression of events between the peaks. The data taken after amplitude modulation (lower graphs Fig. 2d) clearly shows such suppression, with essentially no photon counts present in the regions between successive peaks.

To demonstrate this technique in conjunction with a high repetition rate QD SPS directly, we optically pump the device by an adjustable repetition rate 775 nm source (Fig. 3a) whose trigger output is synchronized to the 980 nm EOM that modulates the generated QD emission. The limit on the useful repetition rate is evident in the bottom right inset of Fig. 3a, which shows how the collected QD emission level scales with repetition rate, in the case of no amplitude modulation. For rates up to 0.5 GHz, the number of collected photons increases nearly linearly, while faster repetition rates are precluded by the dynamics of the QD. Figure 3b shows a measurement of $g^{(2)}(\tau)$ under this 0.5 GHz excitation rate, without modulation (left) and with T_{mod} = 450 ps ± 20 ps (right). The modulated data displays a strong reduction in the overlap between peaks in $g^{(2)}(\tau)$ [see Supplementary Information for additional data]. We also find that suppression of $g^{(2)}(\tau)$ in the regions between the peaks does not necessarily require $T_{mod} < T_1$; the Supplementary Information shows $g^{(2)}(\tau)$ data in which the coincidences between peaks are strongly suppressed even for T_{mod} =1.5 ns > T_1 = 625 ps. In this scenario, amplitude modulation can be a valuable resource in purifying and temporally separating the single photon emission, with an overall transmission level that can be > 60% (Fig. 2c). On the other hand, as we describe in the following section, more aggressive amplitude modulation with $T_{mod} < T_1$ can be used to improve the indistinguishability of the source.

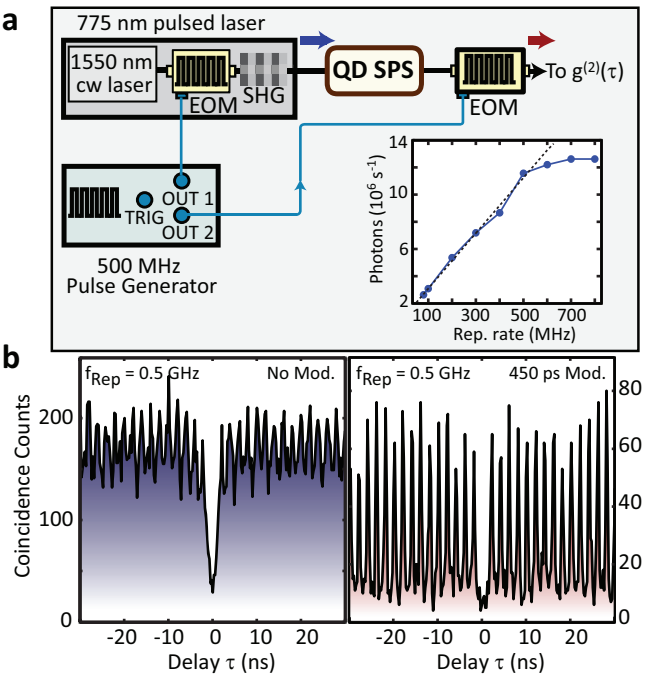

Figure 3 | Towards a GHz repetition rate QD SPS. (a) Setup for generating a 0.5 GHz repetition rate QD SPS. The excitation source is a modulated and frequency doubled 1550 nm laser, producing ≈250 ps width pulses at 775 nm. The pulse generator driving the excitation source synchronously drives the 980 nm EOM to modulate the QD emission. The bottom right inset shows the collected photon count rate from the unmodulated QD SPS as a function of the repetition rate. (b) (left) $g^{(2)}(\tau)$ without modulation. (right) $g^{(2)}(\tau)$ with 450 ps modulation. A clear improvement in the overlap between adjacent peaks in $g^{(2)}(\tau)$ is established after modulation.

Improving the indistinguishability of the single photon source. The generation of indistinguishable photons is an important requirement for several applications in quantum information technology, such as linear optics quantum computing[31], which relies on the two-photon interference effect of single photon pulses at a beamsplitter. When two indistinguishable photons enter a beamsplitter at the same time, they bunch together and leave from the same exit port[22]. This can only be achieved if the photon pulses are Fourier-transform limited, that is, the coherence time (T_2) of the interfering photons is limited only by their radiative lifetime (T_1), such that $V = T_2/(2T_1) = 1$. V quantifies the degree of two-photon wavpacket overlap, and in the limit of a pure SPS ($g^{(2)}(0) = 0$), $V = 1$ implies perfectly indistinguishable photons.

The coherence time of single photons emitted from QDs is limited due to several dephasing processes which reduce their indistinguishability through lower T_2 values. Resonant excitation[13,32,33] and Purcell enhancement can bring the photons closer to the Fourier-transform limit[12,16], through the reduction of dephasing processes and the radiative lifetime, respectively. Electrically-injected structures in which dephasing was filtered out through fast Stark shifting have also been demonstrated[34]. As a new approach that is independent of the specific device geometry and excitation wavelength, here we demonstrate that amplitude modulation can improve the indistinguishability of our SPS through two means. The first is through the improved purity of the SPS, as we have detailed in the previous section. The second is through selection of the coherent portion of the single photon wavepackets, which increases V from $T_2/(2T_1)$ to $T_2/(2T_{mod})$. Conceptually, this is similar to spectral filtering within the homogeneous linewidth of the QD, which has been predicted to improve photon indistinguishability[35].

Figure 4a shows the experimental setup used for photon indistinguishability measurements. For each repetition period of the 832 nm excitation laser, we generate a pair of pulses with a delay $\Delta t = 2.2$ ns, equal to the delay in the HOM interferometer, thus enabling the interference between the consecutively emitted photons. The same delay is introduced to the output of the electronic pulse generator which drives the EOM. For these measurements, we use the same device as in the previous section, but a shift in the spectral position of the cavity mode with respect to the QD transition resulted in a longer radiative lifetime $T_1 = 770$ ps $\pm$ 20 ps, and higher antibunching value $g^{(2)}(0) = 0.29 \pm 0.04$ [data in the Supplementary Information]. Figure 4b shows the result of the HOM measurement on the spectrally filtered QD emission without amplitude modulation. Examining the peak areas $A_{2,3,4}$ results in $M = 0.49$, less than the value $M = 0.61$ expected for the measured $g^{(2)}(0)$ value if there was no two-photon interference.

Next, we performed a HOM measurement after amplitude modulation. We measured $T_{mod} = 380$ ps $\pm$ 20 ps, which is approximately half the QD T_1 value, and suggests that a factor of two increase in V should be expected. We first measured the auto-correlation of the modulated QD emission as $g^{(2)}(0) = 0.20 \pm 0.04$ [see Supplementary Information], again evidencing an improvement in the purity of the SPS. Figure 4c shows the result of the HOM experiment, where the correlation peaks are now well-separated due to the modulation. We estimate $M = 0.31$, which is smaller than the value $M = 0.58$ expected for this device if there was no two-photon interference. Our measured value $M = 0.31$ yields $V = 0.65 \pm 0.06$, which corresponds to a coherence time $T_2 = 500$ ps $\pm$ 50 ps given $T_{mod} \approx$ 380 ps. In comparison, the unmodulated case has $M = 0.49$ and $g^{(2)}(0) = 0.29 \pm 0.04$, which gives an unmodulated value $V = 0.32 \pm 0.05$ that is consistent with the ratio $T_2/2T_1$ for $T_2 \approx$500 ps and $T_1 \approx$770 ps. Thus, the two-photon wavepacket overlap V is increased by a factor of two, as expected based on the change from T_1 to T_{mod} produced by amplitude modulation. V after modulation approaches the value of $\approx$0.8 achieved in previous works[12,14,16] through quasi-resonant excitation and larger Purcell enhancement.

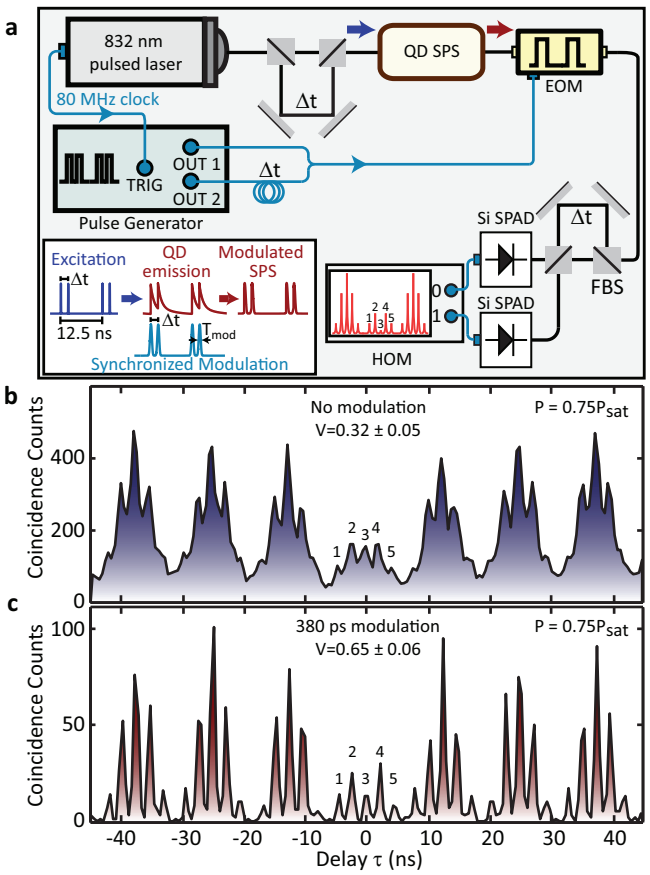

Figure 4 | Improving the indistinguishability of single photons through amplitude modulation. (a) Schematic of the setup for Hong-Ou-Mandel (HOM) interference with and without amplitude modulation. Emission from the QD is sent into a Mach-Zehnder interferometer in which a $\Delta t = 2.2$ ns delay is inserted into one of the arms. The same value of Δt is used in the excitation path and in the dual-channel output of the pulse pattern generator. (b) HOM measurement without amplitude modulation. (c) HOM measurement with 380 ps amplitude modulation. The two-photon wavepacket overlap improves from $V = 0.32 \pm 0.05$ without amplitude modulation to $V = 0.65 \pm 0.06$ with amplitude modulation, in agreement with the prediction based on the reduction from $T_1 = 770$ ps $\pm$ 20 ps to $T_{mod} = 380$ ps $\pm$ 20 ps. The uncertainties in V come from the uncertainty in the measured $g^{(2)}(0)$ values [see Supplementary Information].

Amplitude modulation is fully compatible with such techniques, where shorter T_1 values would result in higher transmission for a fixed T_{mod} (Fig. 2c), and longer T_2 values would improve the indistinguishability.

Discussion

In conclusion, we have demonstrated that synchronous amplitude modulation of QD emission can be an effective approach to improving its performance as a SPS. We first demonstrate a fiber-coupled microcavity-QD SPS which exhibits high brightness but whose application may be limited by imperfect purity and indistinguishability. The temporal filtering provided by the amplitude modulator allows us to select the portions of the emission for which the behavior is more ideal. This results in a significant improvement in the single photon purity of the source, by as much as a factor of 8, and enables clean operation of the SPS up to repetition rates as high as 0.5 GHz. Using amplitude modulation to eliminate portions of the single photon wavepackets that are incoherent improves the two-photon wavepacket overlap by a factor of 2.

Though related in some respects, this work is fundamentally different than experiments which have utilized post-selection in conjunction with triggered sources in order to eliminate detection events outside of a prescribed temporal window[36]; the amplitude modulation is physically filtering the quantum dot emission in time, thereby changing the single photon wavepacket shape and eliminating multi-photon emission and much of the incoherent portion of the single photon wavepacket. For many applications, such as in scalable hybrid quantum information processing, for example, this physical improvement in the source quality is preferable to post-selection. In addition, though our approach necessarily reduces the brightness of the system, efficiencies in excess of 50% can be achieved depending on the needed modulation width. In our experiments, typical efficiencies are 30%; when combined with $>$ 20% collection efficiency and a triggering rate as high as 500 MHz, the overall fiber-coupled flux of single photons can exceed 30 MHz.

We emphasize the versatility of amplitude modulation, as it can be applied to either optically (non-resonant or resonant) or electrically pumped devices, independent of device geometry and the precise energy level structure of the QD. It can also be used in conjunction with other methods that improve the performance of SPSs, such as resonant excitation or Purcell enhancement. Other solid-state quantum emitters, such as nitrogen vacancy centers in diamond[37,38] and colloidal quantum dots[39] often exhibit non-zero multi-photon probability and imperfect two-photon interference; amplitude modulation may be a valuable resource for those systems as well. Finally, the ability to temporally filter the emitted signal with adjustable width and position provides a new resource to help understand the dynamics within mesoscopic quantum systems like single semiconductor quantum dots.

Methods

SPS brightness estimate. The QD SPS efficiency is estimated by comparing the number of photons coupled to the FTW at P_{sat} to the expected number of generated photons. The total detection efficiency of the optical setup ζ includes the transmission through the FTW (50%) and spectral filtering setup (50%) and the quantum efficiency of the SPADs (12.5%), measured using a laser of known power at the QD emission wavelength. Assuming the QD generates one photon per excitation pulse, the efficiency of the QD SPS is given by $\xi = I_{sat}/(R_{Rep} * \zeta)$, where I_{sat} is the detected count rate on the SPAD and R_{Rep} is the 80 MHz repetition rate of the excitation laser. Error bars in the measurements come from the fluctuation in the detected count rates, and are one standard deviation values. The Supplementary Information provides further details in comparing the fiber-coupled brightness of this source with other works.

Indistinguishability measurements. Analysis of the indistinguishability measurements is done following Santori et al.[12]. The mean two-photon overlap V is linked to:

$$M = \frac{A_3}{A_2 + A_4} = \frac{(1+2g^*)}{2(1+g^*)} - \frac{(1-\varepsilon)^2 R^2 T^2 V}{(1+g^*)(R^3T + RT^3)} \quad (1)$$

where A_3 is the area of the central peak and A_2 and A_4 are the areas of the inner side peaks as labeled in Fig. 4b, (1-ε) is the visibility of the interferometer, R and T are the reflectivity and transmission of the beamsplitters, and g^* is the probability of two-photon generation divided by the probability of one photon generation in each pulse; g^* is taken equal to the measured $g^{(2)}(0)$ values. For a pure SPS with $g^{(2)}(0) = 0$, $M = 0$ for perfect interference with $V = 1$, while $M = 0.5$ for no interference ($V = 0$). Considering the different $g^{(2)}(0)$ values measured in Fig. 1e and Fig. 4b and c, the expected M values with no interference are 0.57, 0.58, and 0.61, respectively.

1. Lounis, B. & Orrit, M. Single-photon sources. *Reports on Progress in Physics* **68**, 1129–1179 (2005).
2. Santori, C., Fattal, D. & Yamamoto, Y. *Single-photon Devices and Applications* (Wiley-VCH, Leipzig, 2010).
3. Shields, A. J. Semiconductor quantum light sources. *Nature Photonics* **1**, 215–223 (2007).
4. Michler, P. (ed.) *Single Semiconductor Quantum Dots* (Springer Verlag, Berlin, 2009).
5. Pelton, M. *et al.* Efficient source of single photons: a single quantum dot in a micropost microcavity. *Phys. Rev. Lett.* **89**, 233602 (2002).
6. Solomon, G., Pelton, M. & Yamamoto, Y. Single-mode spontaneous emission from a single quantum dot in a three-dimensional microcavity. *Phys. Rev. Lett.* **86**, 3903–3906 (2001).
7. Strauf, S. *et al.* High-frequency single-photon source with polarization control. *Nature Photonics* **1**, 704–708 (2007).
8. Toishi, M., Englund, D., Faraon, A. & Vuckovic, J. High-brightness single photon source from a quantum dot in a directional-emission nanocavity. *Opt. Express* **17**, 14618–14626 (2009).
9. Claudon, J. *et al.* A highly efficient single-photon source based on a quantum dot in a photonic nanowire. *Nature Photonics* **4**, 174–177 (2010).
10. Davanço, M., Rakher, M. T., Schuh, D., Badolato, A. & Srinivasan, K. A circular dielectric grating for vertical extraction of single quantum dot emission. *Appl. Phys. Lett.* **99**, 041102 (2011).
11. Santori, C., Fattal, D., Vuckovic, J., Solomon, G. S. & Yamamoto, Y. Single-photon generation with InAs quantum dots. *New J. Phys.* **6**, 89 (2004).
12. Santori, C., Fattal, D., Vuckovic, J., Solomon, G. & Yamamoto, Y. Indistinguishable photons from a single-photon device. *Nature* **419**, 594–597 (2002).
13. Ates, S. *et al.* Post-selected indistinguishable photons from the resonance fluorescence of a single quantum dot in a microcavity. *Phys. Rev. Lett.* **103**, 167402 (2009).
14. Weiler, S. *et al.* Highly indistinguishable photons from a quantum dot in a microcavity. *Physica Status Solidi B Basic Research* **248**, 867–871 (2011).
15. Gérard, J.-M. & Gayral, B. Strong Purcell effect for InAs quantum boxes in three-dimensional solid-state microcavities. *J. Lightwave Tech.* **17**, 2089–2095 (1999).
16. Varoutsis, S. *et al.* Restoration of photon indistinguishability in the emission of a semiconductor quantum dot. *Phys. Rev. B* **72**, 041303 (2005).
17. Kolchin, P., Belthangady, C., Du, S., Yin, G. Y. & Harris, S. E. Electro-Optic Modulation of Single Photons. *Phys. Rev. Lett.* **101**, 103601 (2008).
18. Specht, H. P. *et al.* Phase shaping of single-photon wave packets. *Nature Photonics* **3**, 469–472 (2009).
19. Rakher, M. T. & Srinivasan, K. Subnanosecond electro-optic modulation of triggered single photons from a quantum dot. *Appl. Phys. Lett.* **98**, 211103 (2011).
20. Srinivasan, K., Borselli, M., Painter, O., Stintz, A. & Krishna, S. Cavity *Q*, mode volume, and lasing threshold in small diameter AlGaAs microdisks with embedded quantum dots. *Opt. Express* **14**, 1094–1105 (2006).
21. Davanço, M. *et al.* Efficient quantum dot single photon extraction into an optical fiber using a nanophotonic directional coupler. *Appl. Phys. Lett.* **99**, 121101 (2011).
22. Hong, C. K., Ou, Z. Y. & Mandel, L. Measurement of subpicosecond time intervals between two photons by interference. *Phys. Rev. Lett.* **59**, 2044–2046 (1987).
23. Ates, S. *et al.* Two-Photon Interference Using Background-Free Quantum Frequency Conversion of Single Photons Emitted by an InAs Quantum Dot. *Phys. Rev. Lett.* **109**, 147405 (2012).
24. Winger, M. *et al.* Explanation of Photon Correlations in the Far-Off-Resonance Optical Emission from a Quantum - Dot Cavity System. *Phys. Rev. Lett.* **103**, 207403 (2009).
25. Chauvin, N. *et al.* Controlling the charge environment of single quantum dots in a photonic-crystal cavity. *Phys. Rev. B* **80**, 241306 (2009).
26. Laucht, A. *et al.* Temporal monitoring of nonresonant feeding of semiconductor nanocavity modes by quantum dot multiexciton transitions. *Phys. Rev. B* **81**, 241302 (2010).
27. Peter, E. *et al.* Fast radiative quantum dots: From single to multiple photon emission. *Appl. Phys. Lett.* **90**, 223118 (2007).
28. Aichele, T., Zwiller, V. & Benson, O. Visible single-photon generation from semiconductor quantum dots. *New J. Phys.* **6**, 90 (2004).
29. Ellis, D. J. P. *et al.* Cavity-enhanced radiative emission rate in a single-photon-emitting diode operating at 0.5 GHz. *New J. Phys.* **10**, 043035 (2008).
30. Bennett, A. J. *et al.* Electrical control of the uncertainty in the time of single photon emission events. *Phys. Rev. B* **72**, 033316 (2005).
31. Knill, E., Laflamme, R. & Milburn, G. J. A scheme for efficient quantum computation with linear optics. *Nature* **409**, 46–52 (2001).
32. Muller, A. *et al.* Resonance fluorescence from a coherently driven semiconductor quantum dot in a cavity. *Phys. Rev. Lett.* **99**, 187402 (2007).
33. Vamivakas, A. N., Zhao, Y., Lu, C.-Y. & Atatüre, M. Spin-resolved quantum-dot resonance fluorescence. *Nature Physics* **5**, 198–202 (2009).
34. Bennett, A. J. *et al.* Indistinguishable photons from a diode. *Appl. Phys. Lett.* **92**, 193503 (2008).
35. Santori, C., Fattal, D., Fu, K.-M. C., Barclay, P. E. & Beausoleil, R. G. On the indistinguishability of Raman photons. *New J. Phys.* **11**, 123009 (2009).
36. Young, R. J. *et al.* Bell-Inequality Violation with a Triggered Photon-Pair Source. *Phys. Rev. Lett.* **102**, 030406 (2009).
37. Kurtsiefer, C., Mayer, S., Zarda, P. & Weinfurter, H. Stable solid-state source of single photons. *Phys. Rev. Lett.* **85**, 290–293 (2000).
38. Babinec, T. M. *et al.* A diamond nanowire single-photon source. *Nature Nanotechnology* **5**, 195–199 (2010).
39. Sebald, K. *et al.* Single-photon emission of CdSe quantum dots at temperatures up to 200 K. *Appl. Phys. Lett.* **81**, 2920 (2002).

Acknowledgements

S.A. and I.A. acknowledge support under the Cooperative Research Agreement between the University of Maryland and NIST-CNST, Award 70NANB10H193. The authors thank Matthew Rakher for useful discussions and early contributions to this work.

Author contributions

S.A. and K.S. fabricated the devices and A.B. grew the quantum dot material. S.A., I.A. and K.S. performed the measurements, in part using high timing resolution detectors developed by A.G. and I.R. K.S. and S.A. wrote the manuscript, with input from all authors. K.S. supervised the project.

Additional information

Supplementary information accompanies this paper at http://www.nature.com/scientificreports

Competing financial interests: The authors declare no competing financial interests.

How to cite this article: Ates, S. *et al.* Improving the performance of bright quantum dot single photon sources using temporal filtering via amplitude modulation. *Sci. Rep.* **3**, 1397; DOI:10.1038/srep01397 (2013).